Journal of Biomechanics 41 (2008) 3107–3115

Contents lists available at ScienceDirect

Journal of Biomechanics

journal homepage: www.elsevier.com/locate/jbiomech
www.JBiomech.com

Understanding site-specific residual strain and architecture in bovine cortical bone

Bijay Giri, Shigeru Tadano *, Kazuhiro Fujisaki, Masahiro Todoh

Division of Human Mechanical Systems and Design, Graduate School of Engineering, Hokkaido University, Sapporo, Japan

ARTICLE INFO

Article history:
Accepted 15 September 2008

Keywords:
Residual strain
Degree of orientation
Strain adaptation
Foramen
X-ray diffraction

ABSTRACT

Living bone is considered as adaptive material to the mechanical functions, which continually undergoes change in its histological arrangement with respect to external prolonged loading. Such remodeling phenomena within bone depend on the degree of stimuli caused by the mechanical loading being experienced, and therefore, are specific to the sites. In the attempts of understanding strain adaptive phenomena within bones, different theoretical models have been proposed. Also, the existing literatures mostly follow the measurement of surface strains using strain gauges to experimentally quantify the strains experienced in the functional environment. In this work, we propose a novel idea of understanding site-specific functional adaptation to the prolonged load in bone on the basis of inherited residual strains and structural organization. We quantified the residual strains and amount of apatite crystals distribution, i.e., the degree of orientation, using X-ray diffraction procedures. The sites of naturally existing hole in bone, called foramen, are considered from bovine femur and metacarpal samples. Significant values of residual strains are found to exist in the specimens. Trends of residual strains noted in the specimens are mostly consistent with the degree of orientation of the crystallites. These features explain the response behavior of bone to the mechanical loading history near the foramen sites. Preferential orientation of crystals mapped around a femoral foramen specimen showed furnished tailored arrangement of the crystals around the hole. Effect of external loading at the femoral foramen site is also explained by the tensile loading experiment.

1. Introduction

The hierarchical structure of bone has drawn the interest of many researchers due to its enhanced stiffness and strength. This is generally regarded to the two-phase composite nature of bone consisting of apatite minerals (close to hydroxyapatite) and collagen matrix, and their structural organization (Currey, 2005; Fratzl et al., 2004). The interaction of mineral and collagen in bone is still a matter of dispute within the scientific community. Besides the concept of a mineral-reinforced collagen matrix (Currey, 1969; Katz, 1980, 1981; Sasaki et al., 1991), there is also evidence for a mineral matrix with collagen inclusions (Aoubiza et al., 1996; Benezra Rosen et al., 2002; Crolet et al., 1993; Currey, 2008; Hellmich and Ulm, 2002). Moreover, it has recently been proposed (Fritsch and Hellmich, 2007) to reconcile these two seemingly opposed concepts; both are probably relevant for bone, but at different observation scales.

Julius Wolff based on his observations and experimental studies proposed that bone tissue is an adaptable material and that its structural organization and mass have direct relation to the magnitude and direction of forces subjected to it. Intensive studies to provide further lights on the basic idea of functional adaptation of bone continued since then (Cowin, 2006; Ehrlich and Lanyon, 2002; Huiskes, 2000). Bone cells are supposed to be stimulated by the mechanical input, i.e., strain, to adapt to the loading environment they experience. The prolonged strain causes histological adaptation making bone stiffer and dense, whereas lack of sufficient strains may conversely make it less stiff and porous (Huiskes et al., 1987). The adaptation of bone has been explained with different theoretical models and physiological mechanism of cells (Cowin and Doty, 2007; Huiskes et al., 2000). To quantify the strains developed in functional environments, measurement of surface strains using strain gauges are generally conducted (Burr et al., 1996; Fritton and Rubin, 2001; Gross et al., 1992). In this study, we present a different approach of understanding the strains experienced assuming them to be inherited in the bone according to the loading environment it faced.

Since any change is caused by the long-term strain, certain amount of strain is supposed to be inherited within bone depending on the mechanical loading history it experienced. Such strain remains in the form of residual strain. The term ‘residual

* Corresponding author. Tel./fax: +81 11 7066405.
E-mail address: tadano@eng.hokudai.ac.jp (S. Tadano).

0021-9290/$ - see front matter © 2008 Elsevier Ltd. All rights reserved.
doi:10.1016/j.jbiomech.2008.09.012

strain' is normally used in the study of crystalline materials which can have plastic deformation due to dislocation. For biological materials, it may be considered as 'pre-strain'. Study on the residual stress–strain estimation of common engineering materials applying X-ray diffraction method is widespread. In very few applications with bone, the authors have successfully applied X-ray diffraction procedure to quantify residual stresses at the bone surface-Tadano and Okoshi (2006) have reported the existence of residual stress in rabbit tibiofibula and Todoh et al. (2000) have measured the anisotropic residual stress in bovine femoral shaft.

Bone contains holes of varying size throughout the body since the fetal age. Such holes existing for blood vessels and nerves to pass are known as 'foramina' (singular 'foramen'). Unlike normal structures, these foramina are rarely discovered as the site of crack initiation or growth. A single study to address stress concentration around such natural hole reported the distribution of mineral fraction as a main feature to control fracture near foramen (Götzen et al., 2003). In the contrary, in more precise outcomes using X-rays, our study with the complex site of bovine vertebral foramen revealed that the foramen region is reinforced due to regularly organized apatite crystals and added cortical layer around the hole (Giri et al., 2007). The distribution of mineral fraction was unpredictable. In this work, we put forward a concept of quantifying the inherited residual strain as well as the structural feature, i.e., the distribution of apatite crystals in bone. Our purpose is to first observe whether there exists any such strain, and then base it with the orientation distribution factor to relate to the site-specific loading history originally experienced.

We considered different sites of bone natural holes, which exist since the fetal age. A laboratory based two-dimensional X-ray diffraction detector system was used to measure lattice residual strains in cortical bone specimens from the foramen site of bovine metacarpals and femurs. The degree of orientation of apatite crystals with reference to the sample axis was quantified for these sites. We also mapped the two-dimensional distribution of apatite crystals considering their preferred orientation for a femoral foramen. The effect of external loading was also observed. In comparison to the existing works on functional strain quantification at the surfaces, which make use of bulky bone samples in vivo or in vitro, here we considered the approach of inherited residual strains by using samples from the interior bone regions to address the site-specific case of adaptation.

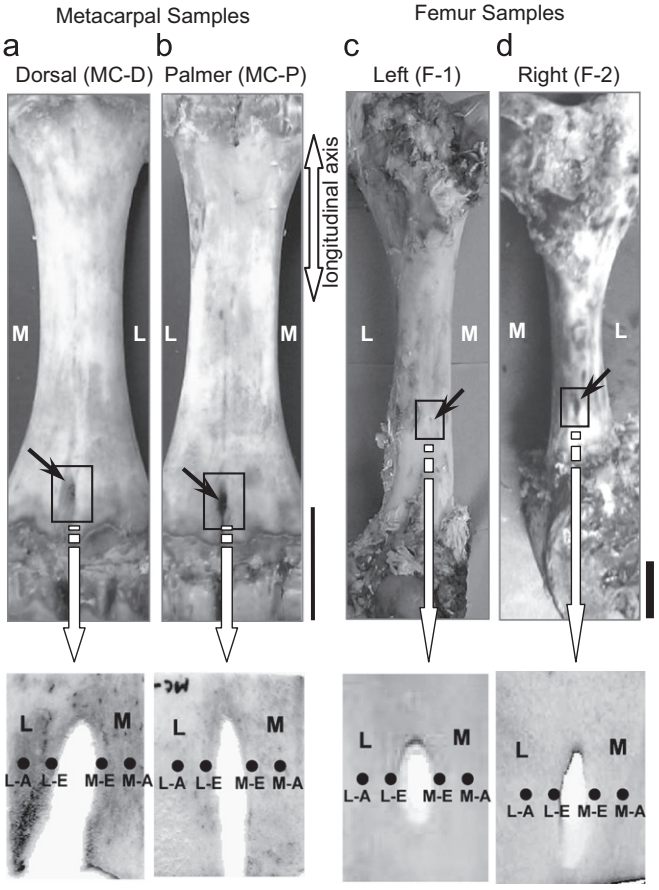

Fig. 1. Metacarpal and femoral samples (*top*). Locations of foramina are shown by arrows. The scale bars are 50 mm. Cortical specimens (approx. 20×15 mm) were harvested from the samples with foramen almost at the center (*bottom*). Femoral foramina lie distally along medial-posterior aspect. Metacarpal foramina lie distally along mid-dorsal and mid-palmer aspects. The measured points are shown in the specimens with the notations to define the locations.

2. Materials and methods

2.1. Specimen

Fresh femur and metacarpal samples were obtained from 24 months old bovine donors and frozen at $-30\,^{\circ}$C until further preparation. The femoral shaft contains an observable elliptical foramen distally along the medial-posterior aspect with major axis aligned along the femoral axis (Fig. 1). The metacarpal sample has foramen towards the distal end both at the mid-dorsal and mid-palmer aspects. Rectangular cortical strips, approximately 20×15 mm with longer side along the longitudinal axis of the samples, were harvested with foramen almost at the center. Two femoral foramen specimens from different limbs and two metacarpal specimens from palmer and dorsal aspects were used for residual strain measurement. Thickness of the prepared specimens was uniform ranging from 0.5 to 0.8 mm among the specimens.

Two more femur specimens were prepared; one was used to map the crystal orientation and another to study the effect of external loads. All the specimens were preserved in a closed pack until they were taken out for the experiment.

2.2. X-ray diffraction imaging system

X-rays with characteristics Mo-Kα, Mo target, wavelength 0.071 nm, tube voltage 40 kV and tube current 40 mA were generated from the X-ray generator (RINT2000, Rigaku Co., Japan). Mo target is generally preferred for better transmission of X-rays. Schematic diffraction phenomenon with the X-ray diffraction imaging system is shown in Fig. 2. X-ray beam was exposed to the specimen using collimator of 0.5 mm diameter for 10 min. The imaging plate (BAS-SR 127×127 mm, Fuji Photo Film Co. Ltd., Japan) was used to detect the radiation transmitted through the specimen placed at 143 mm distance from the specimen. *R*-axis DS3C scanner (Rigaku Co., Japan) was used to readout X-ray intensity detected by the IP to get the two-dimensional X-ray diffraction image. The IP was scanned to obtain the diffraction patterns at 100 μm/pixel resolutions. A typical diffraction pattern recorded by the IP is shown in Fig. 3(a).

The polar binning of pixel intensity data was done in the azimuthal (β) steps of 0.1° to obtain 3600 radial line distributions. The distribution of each radial line was obtained in 1/10 pixels by the weighted-average of intensities in each pixel. The binning was performed for 211 and 002-planes. Diffraction images were obtained at different specimen tilts with 'ω' equal to 90°, 100°, 110° and 120°. All the analyzes of the diffraction patterns were performed using a software program developed in our laboratory.

Experiments were carried out under nearly the identical environmental conditions maintained within the generator (temperature = 19 °C; relative humidity = 55%).

2.3. Degree of orientation

The reflection of 002-plane is often used to characterize the orientation pattern of apatite crystals. The dense arc-shaped intensity region of 002-plane in the diffracted intensity pattern (Fig. 3a) provides the estimate of the preferential orientation of the crystallites *c*-axes. It is also possible to quantify mathematically the degree of orientation (DO) of the crystals about a reference direction (Wilchinsky, 1960). Our direction of interest here is the direction of strain measurement, i.e., the longitudinal direction corresponding to $\beta = 90$–270°,

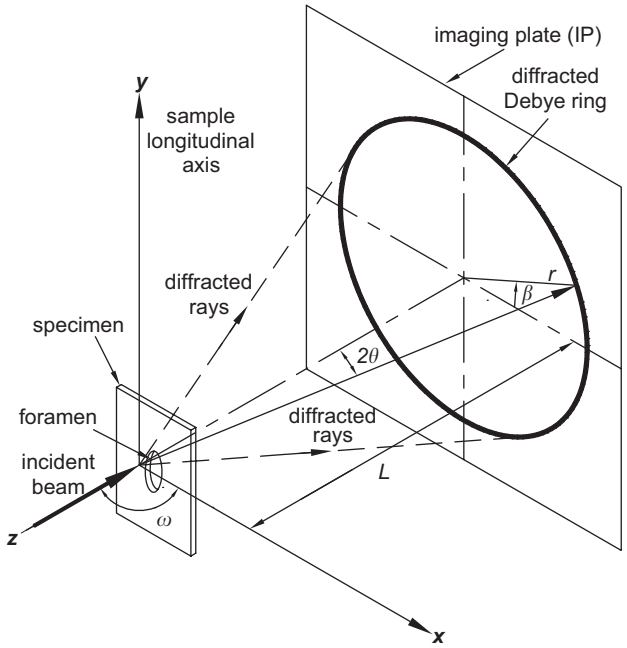

Fig. 2. Schematic of diffraction phenomena in X-ray diffraction imaging-plate system. Symbols are as used in the text.

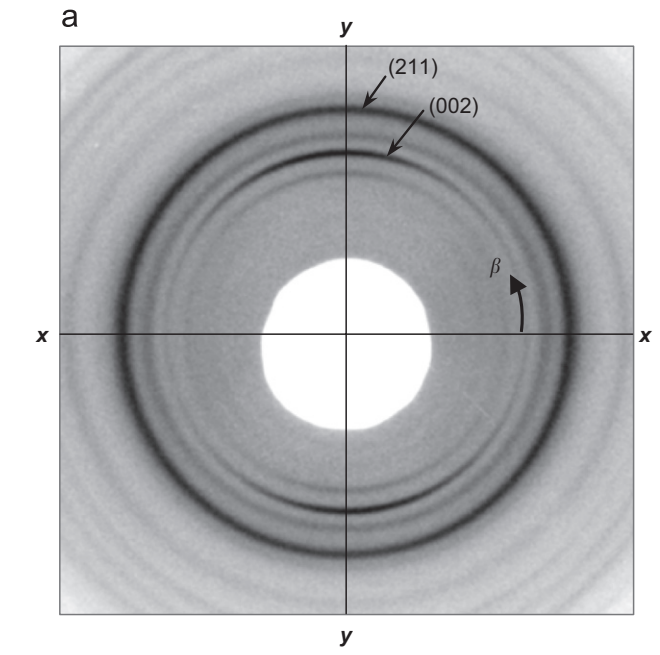

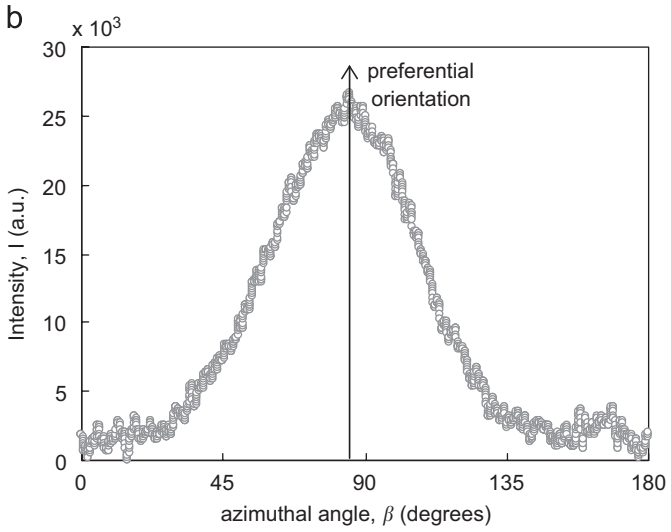

Fig. 3. (a) A sample of two-dimensional intensity distribution profile from IP readout and (b) azimuthal integrated intensity profile of 002-plane. Maximum intensity gives the preferred orientation of the crystals.

and the transverse direction corresponding to $\beta = 0$–180°. The DO expressed as $\langle \cos^2\beta \rangle$ is mathematically obtained using the following equation:

$$\langle \cos^2 \beta \rangle = \frac{\int_0^\pi I(\beta) \cos^2 \beta \sin \beta \, d\beta}{\int_0^\pi I(\beta) \sin \beta \, d\beta} \tag{1}$$

Here, $I(\beta)$ is the intensity at azimuths β. The parameter $\langle \cos^2\beta \rangle$ approaches unity when the alignment of crystals is closer to the reference direction and zero when the crystals are closely aligned perpendicular to the reference direction. Intensities along the radial lines within the annular area enveloping 002-plane were azimuthally integrated at 0.1 degree intervals. The minimum intensity of the azimuthal scan was deducted from the total integrated values, which would give $I(\beta)$ for Eq. (1). A typical integrated intensity profile along 002-plane is shown in Fig. 3(b).

The DOs were calculated for the positions next to the edge of the foramen and away from the foramen at 2 mm distance apart along the medial and lateral sides, respectively. All these positions lie on the same medio-lateral line nearly at the center of the elliptical hole. Diffraction images were recorded for different rotations of the specimens.

Furthermore, the diffraction images were also obtained for a whole femur specimen at 1 mm intervals to map the preferred orientation directions.

2.4. Residual strain

The diffraction profile of 211-plane was considered for strain analysis. Peaks at the full-width-half-maximum (FWHM) of the radial profiles with proper background correction were considered. Diametrically opposite peaks were added to get the diameter of the ring and averaged in 0.5° azimuthal intervals. Relationship between the diffraction data around the whole Debye ring and the lattice strain tensors can be obtained by combining the elastic theory and Bragg's relation for any sample and detector orientation. The detail description of this relationship is found elsewhere (He and Smith, 1997). The fundamental solution of stress–strain has been simplified here to calculate residual strains assuming the plane stress state as shown below;

$$\left(a^2 - \frac{v}{1-v}c^2\right)\varepsilon_{xx} + 2ab\varepsilon_{xy} + \left(b^2 - \frac{v}{1-v}c^2\right)\varepsilon_{yy} + \varepsilon_{ph} = \ln\left(\frac{\sin\theta_0}{\sin\theta}\right) \tag{2}$$

Here,

$a = \sin\theta\cos\omega + \sin\beta\cos\theta\sin\omega$; $\quad b = \cos\beta\cos\theta$;
$c = \sin\theta\sin\omega - \sin\beta\cos\theta\cos\omega$

Since the unstressed specimen state (corresponding to diffraction angle θ_0) is not known, an extra strain component ε_{ph} called pseudo hydrostatic strain needs to be introduced in Eq. (2) for a rough d-spacing. The ideal d-spacing was then calculated by least squares regression of Eq. (2) using the ring diameters of different profile azimuths. The Poisson's ratio $v(=0.29)$ was assumed for the calculation.

Residual strains for both the longitudinal (sample axis) and transverse directions were calculated.

A tensile loading experiment was also performed with a separate femoral foramen specimen under different loading conditions. Lattice strains under loading were calculated according to Eq. (3), derived from Bragg's law ($2d\sin\theta = n\lambda$).

$$\varepsilon_{hkl} = \frac{d - d_0}{d_0} = \frac{\sin\theta_0 - \sin\theta}{\sin\theta} = \frac{\sin\left[\frac{1}{2}\tan^{-1}\left(\frac{r_0}{L}\right)\right] - \sin\left[\frac{1}{2}\tan^{-1}\left(\frac{r}{L}\right)\right]}{\sin\left[\frac{1}{2}\tan^{-1}\left(\frac{r}{L}\right)\right]} \tag{3}$$

Here, d is the interplanar distance, θ is the diffracted angle, r is the radius vector of Debye ring, and L is the sample-detector distance. The subscript '0' indicates values at unstressed (initial) state.

3. Results and discussion

The transmitted intensity patterns obtained in two-dimensional area detectors with the X-ray diffraction imaging system provides much more information about the sample including the knowledge about texture variation. The apatite crystals in bone also possess well-ordered lattice to a larger extent to provide characteristic diffraction patterns with X-rays. The 002-lattice plane of the crystals, which represents *c*-axis orientation, has sharper reflection compared to other planes and provides the tendency of crystallites alignment within the examined area as shown in Fig. 3a and b. Based on the intensity variation of 002-plane, we mathematically quantified the extent of orientation, that is the degree of orientation (DO) at the foramen site. The DOs with reference to the longitudinal direction of the specimens are plotted in Fig. 4.

X-ray pole figure analysis is a widely applied tool in texture characterization (Sasaki et al., 1989; Wagermaier et al., 2006; Wenk and Heidelbach, 1999). The amount of mineral particles together with their shape, size and arrangement are important in determining the mechanical properties of bone composite. The distribution of mineral crystals has been well described from the findings of small-angle X-ray scattering (SAXS) (Fratzl et al., 1992,1996,1997). In a mechanical model of mineralized fibers (Gao et al., 2003; Jäeger and Fratzl, 2000; Ji and Gao, 2004), the importance of geometrical arrangement and length scales of nano-composites have also been emphasized. Here, we obtained the quantified orientation value, which was calculated after deducting the minimum intensity at each azimuthal distribution. This eliminates the isometric fraction leaving only the anisotropic variation of the crystals. The whole azimuthal distribution is thus accounted in the calculation with reference to the direction of interest. The calculated values of DOs for the metacarpal foramen and femoral foramen specimens about the longitudinal direction are also listed in Table 1. The two-dimensional crystallites orientation distributions show the crystals are mostly preferentially aligned along the longitudinal sample axis. The mineralized fibers orientations are also observed to agree with this (Fig. 5). Here, we propose a novel concept by quantifying the inherited strain, i.e., residual strain, and base this with the structural feature, i.e., the orientation distribution of apatite crystals, to address the site-specific deformation characteristics of natural bone holes.

The concentric intensity rings as observed in the diffraction image (Fig. 3a) are perfect circles under ideal conditions, when no external stress–strain exists. These rings generally distort to the elliptical shape during deviatoric deformation of the specimen. Hence, the diameters of these rings are the basis of strain estimation, where the vertical and horizontal diameters give the longitudinal and transverse strains, respectively. The plots of diameter vs $\sin^2\beta$ for the non-rotated specimens are shown in Fig. 6. Under ideal condition, the plot is expected to be a horizontal line; therefore, the slopes in the plots indicate that the rings were distorted due to the existence of residual strains. The 1800 data of diameters along different profile azimuths is a large database to provide the accurate ideal diameter, i.e. unstressed *d*-spacing, resulting in a quicker convergence during regression analysis.

The calculated bone axial and transverse residual strains in the metacarpals and femur samples are plotted in Figs. 7 and 8,

Table 1
Degree of orientation with reference to sample longitudinal axis (mean ± SD)

	Lateral		Medial	
	L–E	L–A	M–E	M–A
MC-D	0.49 ± 0.05	0.52 ± 0.07	0.43 ± 0.03	0.46 ± 0.03
MC-P	0.53 ± 0.04	0.44 ± 0.02	0.42 ± 0.04	0.44 ± 0.05
F-1	0.37 ± 0.03	0.33 ± 0.04	0.42 ± 0.02	0.45 ± 0.03
F-2	0.46 ± 0.03	0.54 ± 0.06	0.44 ± 0.03	0.42 ± 0.01

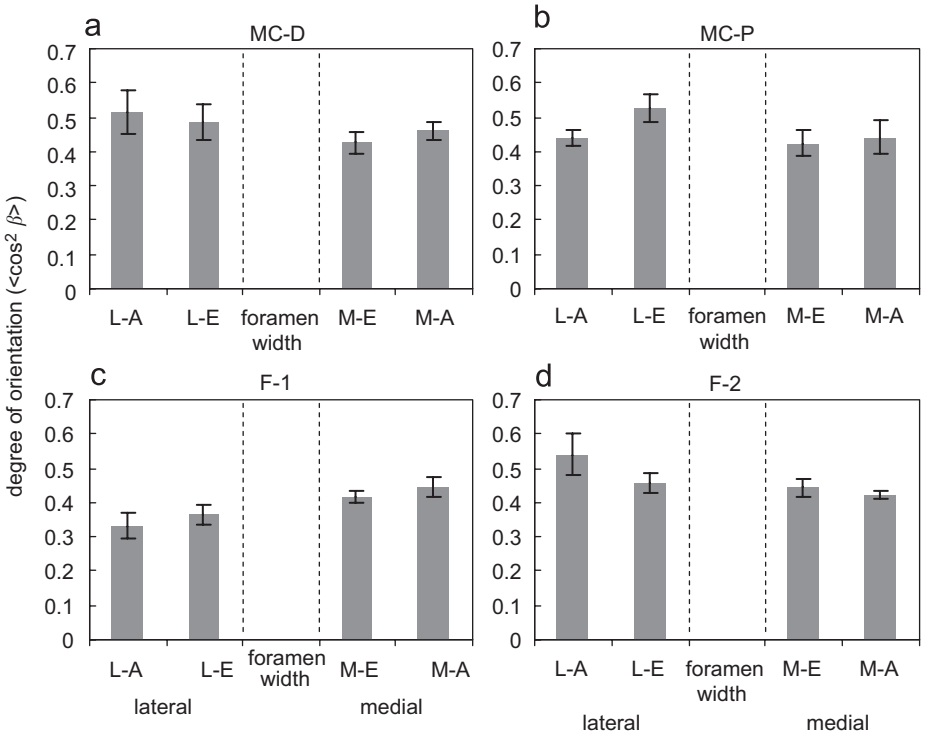

Fig. 4. Degree of orientation (DO) with reference to the sample longitudinal direction ($\beta = 90^\circ$) along lateral and medial of foramen sites for (a) dorsal metacarpal, (b) palmer metacarpal, (c) femur-1, and (d) femur-2. The values are shown for the location next to the foramen edge (L–E, M–E) and away from the edge (L–A, M–A) at 2 mm distance apart.

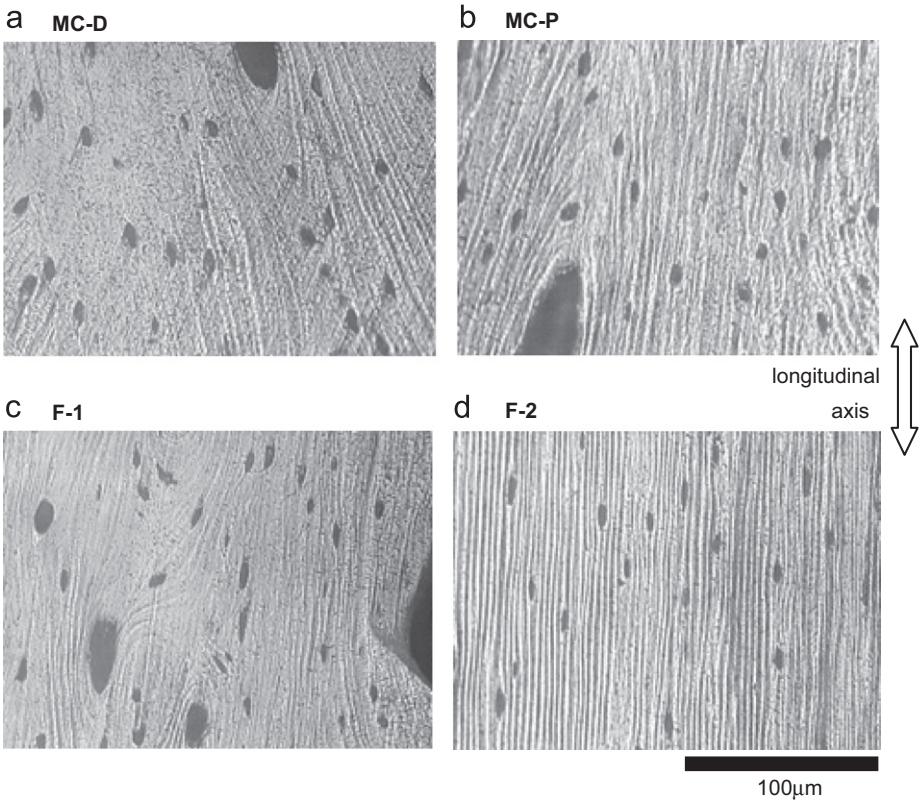

Fig. 5. Microscopic images of (a) dorsal metacarpal, (b) palmer metacarpal, (c) femur-1 and (d) femur-2 specimens near foramen. The fibers are mostly parallel to the sample axis.

respectively. It is expected that higher the concentration of the apatite crystals, the more it is capable to resist the longitudinal load resulting in higher residual strains. The DOs here are mostly consistent with the trend of residual strains in the specimens. The lateral side of palmer metacarpal specimen and femur-2 specimen show higher difference in the residual strains at the edge compared to the far point. These could be regarded to their loading environment and show agreement with the orientation variation of the apatite crystals. The average residual strains in the specimens and the ratio between edge and far values are listed in Table 2. The ratio along longitudinal direction is lower for the lateral side of palmer metacarpal (47%) and femur-2 (61%). Along transverse direction, the ratio is lower for the lateral side of dorsal metacarpal (75%), palmer metacarpal (41%), femur-2 (72%), and the medial side of palmer metacarpal (76%). These sites represent distinct trends.

To see the overall orientation trend at the foramen site, we mapped the preferential orientation of crystals for a femoral foramen specimen. Vectors representing the preferential orientation of crystals are plotted in Fig. 9(a). The alignment of crystals in the femoral foramen sample as expected is longitudinal along the bone axis, but gets diverted as it approaches the foramen region being tangential to the edge. The crystals furnish a tailored structure around the foramen following the hole geometry. Similar alignment tendency of the apatite crystals in the case of vertebral foramen was observed irrespective of the vertebral geometry in our previous work (Fig. 9(b)) (Giri et al., 2007). We further noted slightly different shape of the holes in these two cases; in the femoral foramen, the elliptical shape has elongated major axis dimension (along the bone axis), whereas the vertebral foramen has nearly circular geometry. The difference in the shape of the foramen in these two cases is likely as they are located at different sites within the body. Their shapes are consistent with the locations they exist and the loading history they are expected to experience; the femoral site experiences loads along the bone axis and the vertebral site faces mixed loads. The preferred fiber alignment depends on the mechanical function subjected to the bone (Petrtyl et al., 1996; Riggs et al., 1993). With the local mechanical environment, the principal material direction (the alignment of crystals or collagen fibers) varies to provide ideal strengths to the bone. We can say that according to the varying loading environment bone faces regularly, the extent, orientation and type of the principal strain induced thereby are site-specific as observed here around the foramen.

We also performed a simple tensile loading experiment to understand the external loading effects at the foramen site. The measurements were taken for one of the sides of a femoral foramen specimen next to the foramen edge and away from the edge at 1 and 3 mm distances. These points lie on the same medio-lateral line through the rough center of the elliptical hole. The deformations of two far locations were also measured. At the lower load steps (180 and 220 N), the deformation gradually decreased away from the hole, whereas the positions away from the foramen region (not on the same medio-lateral line) were deformed almost equally with the edge (Fig. 10). On reloading the specimen at the higher load steps (260 and 300 N), the edge was found to deform in a low rate compared to the distant points. The specimen could now be expected to deform uniformly irrespective of the presence of the foramen on further loading.

The mineral crystals in bone are impure form of hydroxyapatite; hence they are considered as poor crystalline material. X-ray diffraction usually requires a rather pure and regular crystal structure to deliver accurate and reliable results. The amount of mineral crystals within the examined area of samples here produced the diffracted intensity patterns, where we assumed that the Debye rings are perfect circles under ideal condition. Any

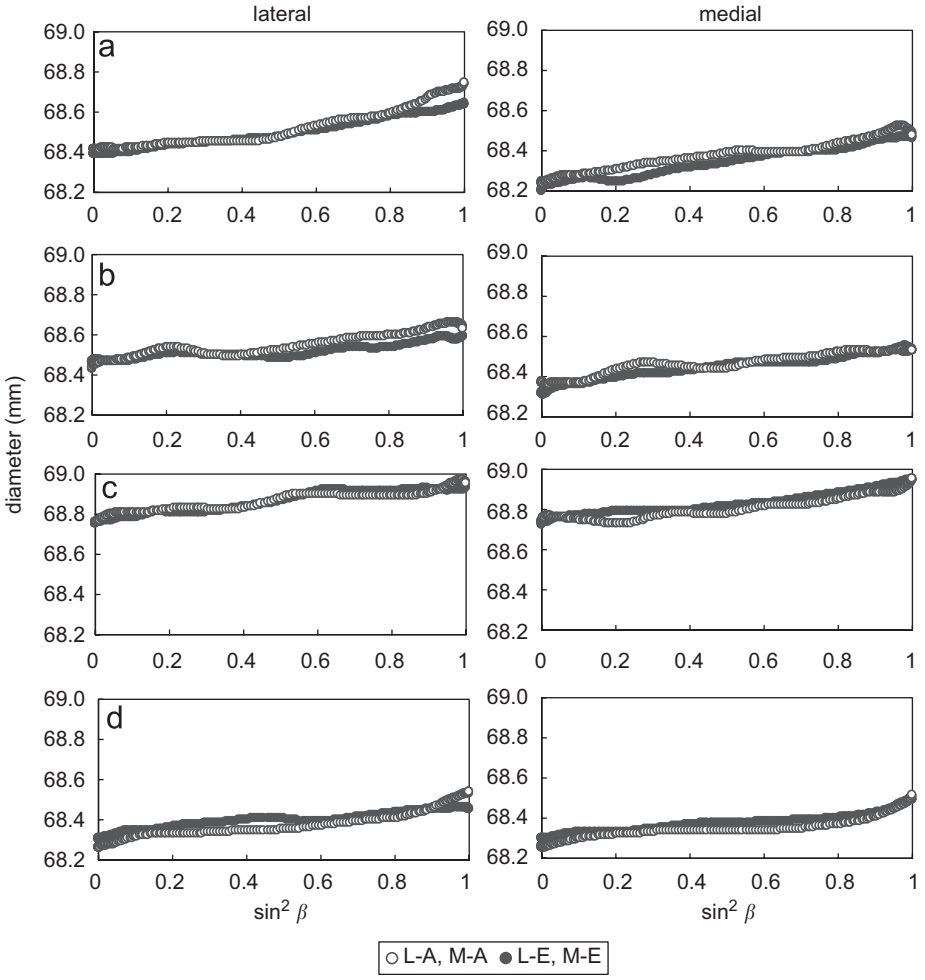

Fig. 6. Representative plots of diameter vs $\sin^2\beta$ (211-plane) along lateral and medial sides of the foramen for (a) dorsal metacarpal, (b) palmer metacarpal, (c) femur-1, and (d) femur-2 at no rotation of the specimens. Slopes in the plots indicate existence of residual strains in all.

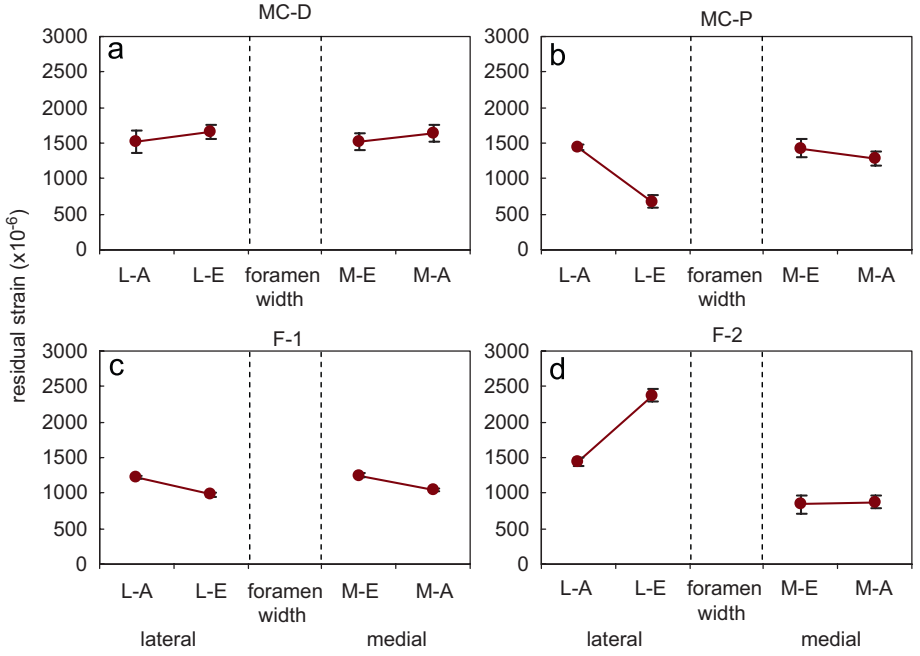

Fig. 7. Lattice residual strains along the longitudinal direction (*yy*) near the foramen region. Locations next to the edge and away from the edge at 2 mm distance were measured along medial and lateral sides. The error bars represent standard deviation for values at different specimen orientations.

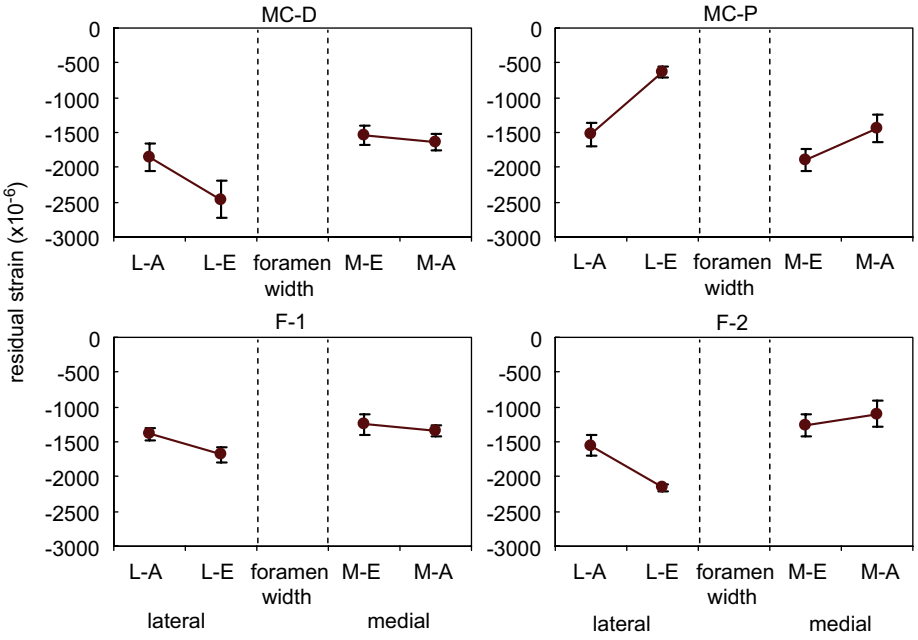

Fig. 8. Lattice residual strains along the transverse direction (*xx*). The error bars represent standard deviation for values at different specimen orientations.

Table 2
Average residual strains along two orthogonal directions

	Longitudinal direction (*yy*)				Transverse direction (*xx*)			
	Lateral		Medial		Lateral		Medial	
	Average strain ($\times 10^{-6}$)	Average strain ratio	Average strain ($\times 10^{-6}$)	Average strain ratio	Average strain ($\times 10^{-6}$)	Average strain ratio	Average strain ($\times 10^{-6}$)	Average strain ratio
MC–D	1589.93	0.91	1581.49	0.92	−2156.62	0.75	−1588.50	0.93
MC–P	1057.50	0.47	1358.89	0.90	−1076.14	0.41	−1665.30	0.76
F-1	1100.61	0.80	1148.68	0.84	−1536.49	0.82	−1294.43	0.93
F-2	1907.96	0.61	858.05	0.97	−1856.35	0.72	−1176.83	0.88

possibility of the effect of un-perfect crystal structure on the quantified residual strain has not been considered. Since the profile is broadened for low crystalline materials like bone, consideration of peak position may not assure accuracy in strain calculation. In such case, accounting the distribution of profile as a whole is expected to provide more accurate results (like FWHM in this case). The authors have also proposed an alternative method and discussed this issue (Fujisaki and Tadano, 2007; Fujisaki et al., 2006; Tadano et al., 2008). Furthermore, the protein present in biocomposite plays an important role in the organization of mineral crystals (Ji and Gao, 2004). In this work, our entire analyzes are based on the mineral crystals and we have not taken into account the effect of presence of protein.

The femoral and metacarpal foramen specimens we prepared were located at different sites of the samples. These specimens were harvested as thin strips from the different depths of bone shaft to allow the transmission of X-rays. Therefore, the differences in the residual strain trends in the specimens at different locations are obvious owing to the long-term load history in different lamella. We carried out experiments with the preserved specimens immediately to reduce the possibility of any significant change in the specimens. However, there are also ways to improve in vitro experimental condition. The experimental and the analysis procedures carried out with the X-ray diffraction system could further be improved as discussed in Tadano et al. (2008).

The knowledge of load distribution in different parts and interior segments of bone and corresponding deformation gradients will assist the researchers in more efficient and precise analysis of the functional adaptation of bone. Besides the measurement precisions, there are other limitations associated with the existing approach of using strain gauges, such as the availability of attachment area, bonding effects, measurement repeatability, and output accuracy in highly local strain change environment. Hence, understanding the inherited strain in bone (measured as residual strain) and their relation with the crystallites orientation using X-ray diffraction techniques provides a better alternative with nano-level understanding of bone functional adaptation. The idea explained here may also be helpful in addressing the physiology of species. Furthermore, the structural information of self-reinforced foramen site in bone can be mimicked to provide solution for engineering structures.

4. Conclusion

Among the various instances of remodeling responses, the current study presents a new concept of understanding site-specific functional adaptation at the nano-scale level with architectural arrangement and strain response to the loading environment. The study considered the case of naturally existing holes in bone, foramina, which exists since the fetal age of species.

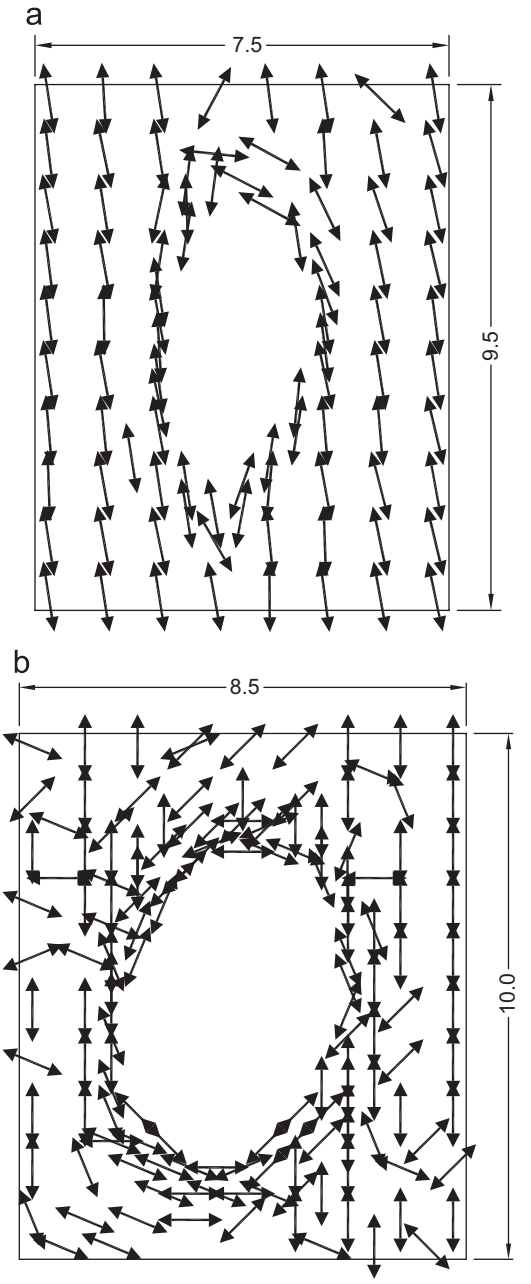

Fig. 9. (a) Mapping of crystallites preferential orientation around the femoral foramen determined from the diffracted intensity values of 002-plane. The crystals are diverted around the edge according to the geometry of the hole. (b) Orientation of the crystals around bovine vertebral foramen with similar tendency (reprinted from Giri et al., 2007).

The study is based on the idea that information about inherited strain, i.e., residual strain and the corresponding structural arrangement is related to the bone adaptation or long-term loading history. We confirmed the existence of significant amount of residual strains in the bone samples, and showed that their tendencies are linked with the extent of mineral crystals. Combining current methodology with the cellular level mechanism, the current state-of-the-art to the bone remodeling approach could be advanced. The study suggests the correlation between crystallites orientation and strains to be taken into account precisely. Hoping such relationship to be interesting and useful to analyze different aspects of complex bone tissue, the authors are underway investigating the effects of external loads to these features.

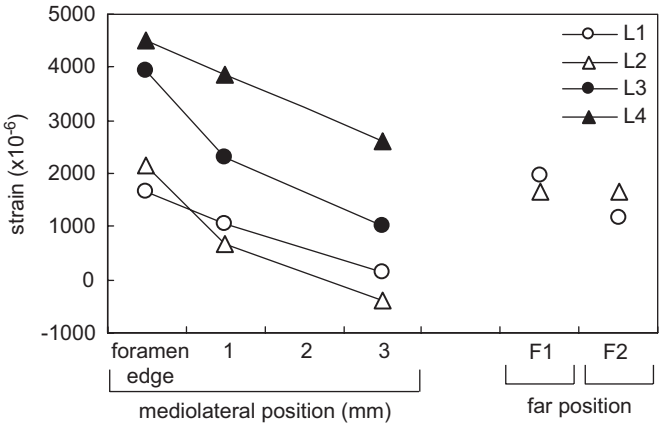

Fig. 10. Lattice strains at different loading stages ($L1 = 180$ N, $L2 = 220$ N, $L3 = 260$ N, $L4 = 300$ N). Deformations were measured at three locations along the same medio-lateral line for lower load steps and higher load steps. Two locations far from the foramen were also measured for lower load steps.

Conflict of interest statement

No actual or potential conflicts of interest exist.

Acknowledgement

This work was supported by Grant-in-Aid for Scientific Research (A), MEXT (No. 19200035).

References

Aoubiza, B., Crolet, J.M., Meunier, A., 1996. On the mechanical characterization of compact bone structure using the homogenization theory. Journal of Biomechanics 29, 1539–1547.

Benezra Rosen, V., Hobbs, L.W., Spector, M., 2002. The ultrastructure of anorganic bovine bone and selected synthetic hydroxyapatites used as bone graft substitute material. Biomaterials 23, 921–928.

Burr, D.B., Milgrom, C., Fyhrie, D., Forwood, M., Nyska, M., Finestone, A., Hoshaw, S., Saiag, E., Simkin, A., 1996. In vivo measurement of human tibial strains during vigorous activity. Bone 18, 405–410.

Cowin, S.C., 2006. The exact stimulus for the strain adaptation of bone tissue is unknown. Journal of Biomechanical Science and Engineering 1, 16–28.

Cowin, S.C., Doty, S.B., 2007. Tissue Mechanics. Springer Science+Bussiness Media, LLC.

Crolet, J.M., Aoubiza, B., Meunier, A., 1993. Compact bone: numerical simulation of mechanical characteristics. Journal of Biomechanics 26, 677–687.

Currey, J.D., 1969. The relationship between the stiffness and the mineral content of bone. Journal of Biomechanics 2, 477–480.

Currey, J.D., 2005. Hierarchies in biomineral structures. Science 309, 253–254.

Currey, J.D., 2008. Collagen and the mechanical properties of bone and calcified cartilage. In: Fratzl, P. (Ed.), Collagen. Springer, New York, pp. 397–420.

Ehrlich, P.J., Lanyon, L.E., 2002. Mechanical strain and bone cell function: a review. Osteoporosis International 13, 688–700.

Fratzl, P., Groschner, M., Vogl, G., Plenk Jr., H., Eschberger, J., Fratzl-Zelman, N., Koller, K., Klaushofer, K., 1992. Mineral crystals in calcified tissues: a comparative study by SAXS. Journal of Bone and Mineral Research 7, 329–334.

Fratzl, P., Schreiber, S., Klaushofer, K., 1996. Bone mineralization as studied by small-angle X-ray scattering. Connective Tissue Research 34, 247–254.

Fratzl, P., Jakob, H.F., Rinnerthaler, S., Roschger, P., Klaushofer, K., 1997. Position-resolved small-angle X-ray scattering of complex biological materials. Journal of Applied Crystallography 30, 765–769.

Fratzl, P., Gupta, H.S., Paschalis, E.P., Roschger, P., 2004. Structure and mechanical quality of the collagen-mineral nano-composite in bone. Journal of Materials Chemistry 14, 2115–2123.

Fritsch, A., Hellmich, Ch., 2007. 'Universal' microstructural patterns in cortical and trabecular, extracellular and extravascular bone materials: micromechanics-based prediction of anisotropic elasticity. Journal of Theoretical Biology 244, 597–620.

Fritton, S.P., Rubin, C.T., 2001. Bone Mechanics Handbook. In: Cowin, S.C. (Ed.), In vivo measurement of bone deformations using strain gauges. CRC Press, Boca Raton, pp. 8-10–8-34.

Fujisaki, K., Tadano, S., 2007. Relationship between bone tissue strain and lattice strain of HAp crystals in bovine cortical bone under tensile loading. Journal of Biomechanics 40, 1832–1838.
Fujisaki, K., Tadano, S., Sasaki, N., 2006. A method on strain measurement of HAp in cortical bone from diffusive profile of X-ray diffraction. Journal of Biomechanics 39, 579–586.
Gao, H., Ji, B., Jäger, I.L., Arzt, E., Fratzl, P., 2003. Materials become insensitive to flaws at nanoscale: lessons from nature. PNAS 100, 5597–5600.
Giri, B., Tadano, S., Fujisaki, K., Todoh, M., 2007. Microstructure of bone around natural hole in bovine lumbar vertebra. Journal of Biomechanical Science and Engineering 2, 1–11.
Götzen, N., Cross, A.R., Ifju, P.G., Rapoff, A.J., 2003. Understanding stress concentration about nutrient foramen. Journal of Biomechanics 36, 1511–1521.
Gross, T.S., McLeod, K.J., Rubin, C.T., 1992. Characterizing bone strain distributions in vivo using three triple rosette strain gages. Journal of Biomechanics 25, 1081–1087.
He, B.B., Smith, K.L., 1997. Strain and stress measurements with a two-dimensional detector. Advances in X-ray Analysis 41, 501–508.
Hellmich, Ch., Ulm, F.-J., 2002. Are mineralized tissues open crystal foams reinforced by crosslinked collagen?—some energy arguments. Journal of Biomechanics 35, 1199–1212.
Huiskes, R., 2000. If bone is the answer, then what is the question? Journal of Anatomy 197, 145–156.
Huiskes, R., Weinans, H., Grootenboer, H.J., Dalstra, M., Fudala, B., Sloof, T.J., 1987. Adaptive bone-remodeling theory applied to prosthetic-design analysis. Journal of Biomechanics 20, 1135–1150.
Huiskes, R., Ruimerman, R., Lenthe, G.H.V., Janssen, J.D., 2000. Effects of mechanical forces on maintenance and adaptation of form in trabecular bone. Nature 405, 704–706.
Jäger, I., Fratzl, P., 2000. Mineralized collagen fibrils: a mechanical model with a staggered arrangement of mineral particles. Biophysical Journal 79, 1737–1746.
Ji, B., Gao, H., 2004. Mechanical properties of nanostructure of biological materials. Journal of the Mechanics and Physics of Solids 52, 1963–1990.
Katz, J.L., 1980. Anisotropy of Young's modulus of bone. Nature 283, 106–107.
Katz, J.L., 1981. Composite material models for cortical bone. American Society of Mechanical Engineers, New York, pp. 171–184.
Petrtyl, M., Hert, J., Fiala, P., 1996. Spatial organization of the haversian bone in man. Journal of Biomechanics 29, 161–169.
Riggs, C.M., Lanyon, L.E., Boyde, A., 1993. Functional associations between collagen fibre orientation and locomotor strain direction in cortical bone of the equine radius. Anatomy and Embryology 187, 231–238.
Sasaki, N., Matsushima, N., Ikawa, T., Yamamura, H., Fukuda, A., 1989. Orientation of bone mineral and its role in the anisotropic mechanical properties of bone-transverse anisotropy. Journal of Biomechanics 22, 157–164.
Sasaki, N., Ikawa, T., Fukuda, A., 1991. Orientation of mineral in bovine bone and the anisotropic mechanical properties of plexiform bone. Journal of Biomechanics 24, 57–61.
Tadano, S., Okoshi, T., 2006. Residual stress in bone structure and tissue of rabbit's tibiofibula. Bio-Medical Materials and Engineering 16, 11–21.
Tadano, S., Giri, B., Takuya, S., Fujisaki, K., Todoh, M., 2008. Estimating nanoscale deformation in bone by X-ray diffraction imaging method. Journal of Biomechanics 41, 945–952.
Todoh, M., Tadano, S., Shibano, J., Ukai, T., 2000. Polychromatic X-ray measurements of anisotropic residual stress in bovine femoral bone. JSME International Journal Series 43, 795–801.
Wagermaier, W., Gupta, H.S., Gourrier, A., Paris, O., Roschger, P., Burghammer, M., Riekel, C., Fratzl, P., 2006. Scanning texture analysis of lamellar bone using microbeam synchrotron X-ray radiation. Journal of Applied Crystallography 40, 115–120.
Wenk, H.R., Heidelbach, F., 1999. Crystal alignment of carbonated apatite in bone and calcified tendon: results from quantitative texture analysis. Bone 24, 361–369.
Wilchinsky, Z.W., 1960. Measurement of orientation in polypropylene film. Journal of Applied Physics 31, 1969–1972.